MICA Optical: A Low-cost, Educational Michelson Interferometer

by

Jillian M. Oliveira

Submitted to the Department of Mechanical Engineering
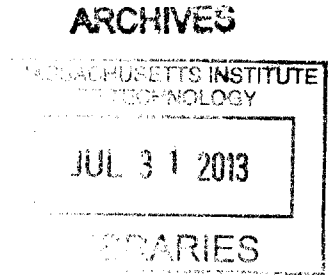in partial fulfillment of the requirements for the degree of

Bachelor of Science in Mechanical Engineering

at the

MASSACHUSETTS INSTITUTE OF TECHNOLOGY

June 2013

—

Author ....
Department of Mechanical Engineering
May 10, 2013

Certified by ....
Ian W. Hunter
Hatsopoulos Professor of Mechanical Engineering
Thesis Supervisor

Accepted by ....
Annette Hosoi
Professor of Mechanical Engineering
Undergraduate Officer

MICA Optical: A Low-cost, Educational Michelson Interferometer

by

Jillian M. Oliveira

Submitted to the Department of Mechanical Engineering
on May 10, 2013, in partial fulfillment of the
requirements for the degree of
Bachelor of Science in Mechanical Engineering

Abstract

Current initiatives that provide widespread access to online educational tools, such as edX and Coursera, are transforming education. The MICA (Measurement, Instrumentation, Control, and Analysis) Project, developed by MIT's BioInstrumentation Lab, is a similar initiative that aims to provide students with affordable, modular, and practical experimental tools. This thesis outlines the development of a MICA optical project, the Michelson interferometer. In this classic experiment, by correctly assembling and aligning the optical components, two different interference patterns can be obtained and observed. Other potential experiments include the measurement of light wavelengths, coherence length, as well as thermal expansion coefficients with the addition of a few simple parts. The initial benchmarking, the design process, and the final manufacturing methods for this module are discussed. The result of this project is a modular kit that can accompany a student's online course materials for about the cost of a textbook.

Thesis Supervisor: Ian W. Hunter
Title: Hatsopoulos Professor of Mechanical Engineering

Acknowledgments

I would like to thank Professor Hunter and the members of the BioInstrumentation Lab. First, I would like to thank Professor Hunter for serving as my thesis supervisor and my UROP (Undergraduate Research Opportunities Program) supervisor, and for providing expertise, leadership, and guidance throughout my research. I would also like to thank Ellen Yi Chen for her unwavering mentorship, supervision, support, and help in lab throughout my thesis and my undergraduate research. It has been an immense opportunity to work with such a talented researcher during my undergraduate years.

I would also like to thank Alison Cloutier for her machine expertise, as well as the other members of the BioInstrumentation Lab for their help in lab. I also would like to extend my appreciation to Kate Melvin for her support and help with purchasing.

Lastly, I would also like to thank my parents, family, and friends for supporting me and believing in me throughout my undergraduate research.

Contents

List of Figures

List of Tables

Chapter 1

Introduction

1.1 The Online Educational Initiative

Science and engineering education often involves hands-on laboratory experiments. In these experiments, students learn to use laboratory apparatuses while also learning about data collection and analysis [1]. Over the past few years, online educational initiatives have been changing the way we think about education. A new online educational program, edX, is a non-profit enterprise founded by Harvard and MIT that offers their class materials online. The goal of edX is to make university education available not only to students present at these institutions, but also to students of "all ages, means, and nations" [2].

MICA, a wireless data acquisition system, is an educational initiative developed by the MIT BioInstrumentation Lab. MICA nodes are packaged in 25 mm cubes so that they can complement online educational initiatives such as edX. MICA educational kits, by utilizing economies of scale, can be sold to students to accompany their online classes for about the cost of a textbook. With MICA, edX courses can integrate laboratory experiments into their curriculum, overcoming a major limitation of online courses and increasing the students' depth of learning [3].

1.2 MICA Optical

The MICA Project, due to its modular nature, can expand into various scientific and engineering disciplines. One area that is currently lacking for MICA is the field of optics. The Michelson Interferometer, a simple laser interferometer setup that consists of basic optical components including a laser, lens(es), a beamsplitter, and mirrors, will complement existing MICA modules. The corresponding experiments demonstrate the basics of optical interferometry by forming a fringe pattern. Students can also learn how to correctly align optical components and perform several measurements with the single Michelson setup. Currently, optical components and mounting devices have extremely high precision, and are therefore too expensive for an individual student learner. However, by designing and manufacturing smaller, simpler components and including low-cost, moderate precision optical components, a similar MICA optical educational kit can be sold to online students at a reasonable cost.

Chapter 2

Background

2.1 MICA

The MICA nodes, shown in Figure 2-1, are packaged as 25 mm cubes and consist of a folded PCB board that houses a processor subsystem, a power management subsystem, and a sensor and generator subsystem. A standard type-B USB port is included for charging and communication, and a LED display presents real time sensor values, graphics, and instructions for the user. Each MICA cube houses a unique sensor module on one or more faces. Sensors contained in the modules built to date include a 16-bit analog to digital converter, a temperature/relative humidity/barometric pressure sensor, a GPS receiver, a 17-bit thermopile, a magnetic field sensor, and a module that allows the other educational sensors to be accessed wirelessly. The MICA cube not only collects and transmits information wirelessly, but it can also record input and output variables simultaneously, which increases the complexity of the experiments and allows students to implement feedback systems and control in their experiments.

2.2 The Michelson interferometer

The Michelson interferometer is a common configuration for optical interferometry. A laser's collimated light is diverged into a larger beam by a diverging lens. The
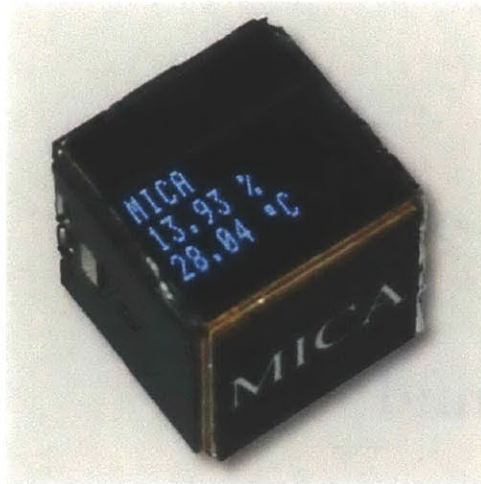
Figure 2-1: MICA cube and LED screen displaying real-time sensor values of relative humidity and temperature [3]

beam is then split into two separate paths by a beamsplitter, where 50% of the beam travels to one mirror and the second 50% travels to another mirror. The two beams recombine at the beamsplitter and the interference pattern is then displayed on a viewing screen [4, 5]. The setup is shown in Figure 2-2. As shown in the figure, the reflection at the beamsplitter produces an image M2' of the mirror M2. The virtual sources S1 and S2 are the images of the original source from the first and second mirrors. The interference pattern is dependent on the nature of the source and the relative positions of M1 and M2'. In one configuration, the source is a collimated laser that is extended through a diverging lens. In this configuration, if the mirrors are perpendicular to each other, as in Figure 2-2a, the interference fringes are circular. If the mirrors are at slight angles to one another, as in Figure 2-2b, the fringes are hyperbolas. In a second configuration, the diverging lens is placed on the other side of the beamsplitter. In this configuration, if the mirrors are perpendicular, the fringes are parallel straight lines [6].

16
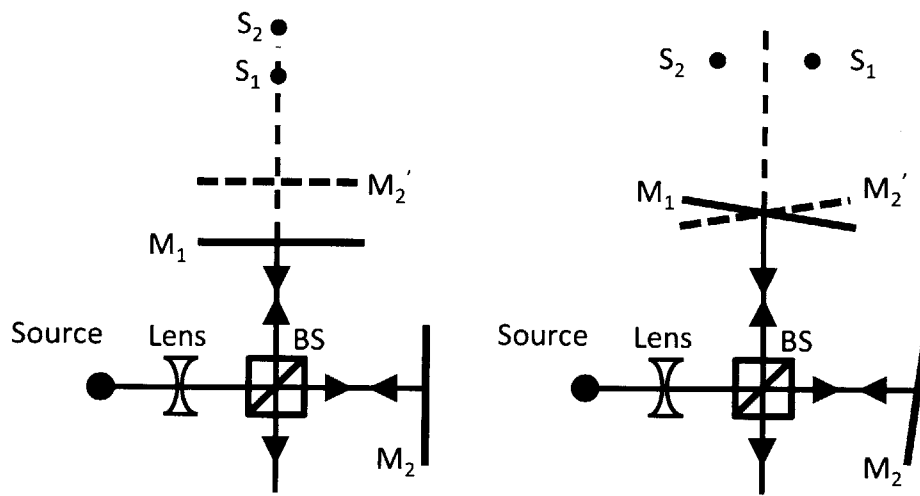
Figure 2-2: The Michelson Interferometer a.) Perpendicular mirrors result in circular fringes b.) Mirrors at slight angles result in parabolic fringes (adapted from [6])

Chapter 3

Theory

3.1 The Michelson Interferometer

3.1.1 Light characteristics

Coherent green laser light from a diode pumped solid state laser travels as a sinusoidal wave with a wavelength, λ, of 532 nm. Given that light travels at c, or approximately 3×10^8 m/s, the frequency, f, of green visible light is approximately 5.6×10^{14} Hz. The amplitude of the wave, A, at any point in time, t, is given by the equation

$$A \propto \sin(2\pi f t). \tag{3.1}$$

Due to its high frequency, light intensity is observed not as a sinusoidal wave, but as a single intensity, or the mean square amplitude, given as

$$I \propto f \int_0^{\frac{1}{f}} A^2 \, dt. \tag{3.2}$$

Although it is not possible to observe the sinusoidal nature of the wave in time, it is possible to observe it in space. This is done by recombining the two light paths with a Michelson interferometer and viewing the interference pattern.

19

3.1.2 Formation of interference pattern

In the first configuration of the Michelson interferometer, described in section 2.2, the light beam from the laser passes through a diverging lens such that the difference in path lengths, ΔX, is given by the equation

$$\Delta X = 2(X_1 - X_2)\cos\theta, \tag{3.3}$$

where θ is the divergence angle, X_1 is the distance from the beamsplitter to the first mirror mount and X_2 is the distance from the beamsplitter to the second mirror mount. This difference in path length, ΔX, can be thought of also as a difference in time, Δt, given that light travels at c.

Given that the first mirror of the interferometer is slightly further from the beam splitter than the second mirror, the amplitudes of the two light paths, A_1 and A_2 are out of phase when recombined at the beamsplitter such that

$$A_1 = \sin(2\pi f t) \quad A_2 = \sin(2\pi f(t + \Delta t)). \tag{3.4}$$

Using equation 3.2 above, the intensity of the resulting beam simplifies to

$$I_{sum} = \frac{1}{2}\cos^2(\frac{\pi\Delta X}{\lambda}). \tag{3.5}$$

The graph of intensity as a function of angle is shown in Figure 3-1. The maximum intensity values correspond to the light fringes in the interference pattern, which occur when the two light beams are in phase. This is constructive interference, and occurs when the path difference is an even multiple of $\lambda/2$. The minimum points of intensity correspond to the dark fringes, which occur when the two light beams are out of phase. This is destructive interference, and occurs when the path length difference is an odd multiple of $\lambda/2$ [7, 8].
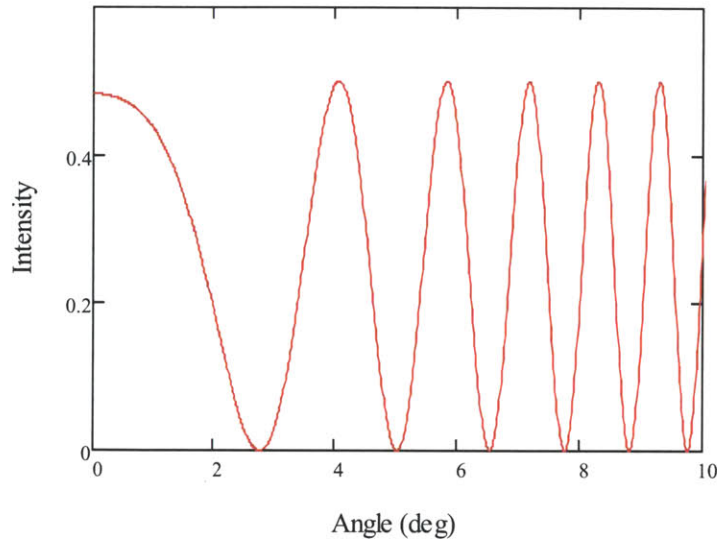
Figure 3-1: Fringe intensity as a function of angle. Points of maximum intensity occur when the two light beams are in phase, occurring when the path difference is an even multiple of $\lambda/2$. The minimum points of intensity occur when the two light beams are out of phase, occurring when the path length difference is an odd multiple of $\lambda/2$

3.2 Flexures

A flexure is a mechanism that produces defined linear and/or angular displacements upon a force application [9]. There are many benefits for flexures. First and foremost, flexures are simple and relatively inexpensive to manufacture. In addition, the small displacements produced by flexures are smooth and continuous with predictable and repetitive motions. There are two types of flexures that produce bending in one axis and are applicable for the Michelson interferometer mirror mounts: the leaf-type spring and the notch hinge, shown in Figure 3-2. The first type, the leaf-type spring, is the most popular flexure element. It is described as a cantilever beam, and it follows general beam bending principles. It can be made from a single body structure or by clamping. The second type, a notch hinge, is the next most popular flexural element, and it is more complex than the leaf-type spring. The notch hinge can be circular or elliptical and therefore requires more complex machining, such as wire electrical discharge machining (EDM) or computer numerical control (CNC) machining. Both

21

of these designs would be applicable for the mirror mounts, but the leaf-type spring was implemented due to its simple manufacturing methods.
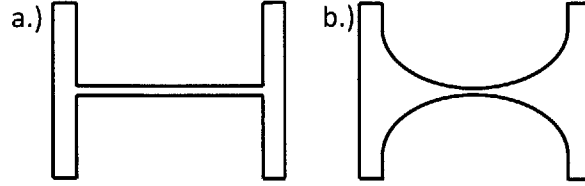
Figure 3-2: Two different types of flexures a.) Leaf-type spring b.) Notch hinge

As the leaf-spring flexure element can be analyzed in terms of beam bending, stiffness and yield stress are critical properties. The angular stiffness of the leaf-type flexure is given by the equation

$$K_\theta = \frac{F_y}{\theta_z} = \frac{2EI}{L^2},$$

(3.6)

where F_y is the downward force on the tip of the beam, θ_z is the angle of deflection, E is the young's modulus, L is the length, and I is the moment of inertia [9]. Given that the length of the flexure is 5 mm, a graph of angular stiffness as a function of thickness is shown in Figure 3-3 for three materials: Aluminum 6061, Stainless Steel 304, and Spring Steel 1074/1075.

As shown in the graph, stainless steel and spring steel's stiffness are more ideal for flexure design.

Yield stress occurs when these three metals reach 1-2% of its permanent stain, or can be defined as the maximum stress at which the stress-stain characteristics deviate from the elastic regime. Therefore, with higher yield stress, the flexure would have a larger elastic regime. The expression below relates the yield stress to the geometry of the flexure.

$$h = \frac{2L\sigma_y}{E\theta_{max}},$$

(3.7)

where h is the thickness of the flexure, θ_{max} is the maximum deflection angle, and
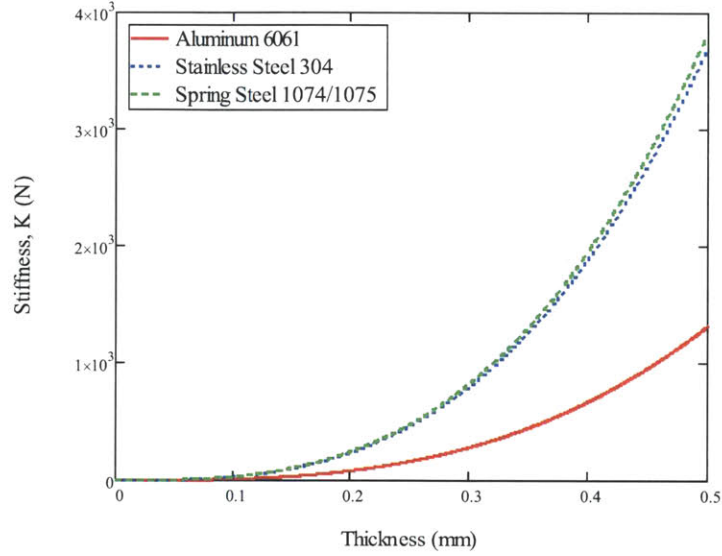
Figure 3-3: Angular stiffness of a leaf-type spring flexure as a function of thickness for Aluminum 6061, Stainless Steel 304, and Spring Steel 1074/1075

σ_y is the yield stress [9]. It was determined that from a maximum length of 5 mm, and a thickness of 0.35 mm, the flexure would begin to deform plastically around a 2 degree angle for general stainless steel and around 4 degrees around spring steel. Figure 3-4 shows a graph of stress as a function of angle.

Since the device was manufactured from stainless steel as described in section 4.3.2, the device was preloaded past -2.5 degrees in order to allow for springback to return the plates to a negative inital angle. The equation below gives a relationship between the initial angle before springback, θ_i, and the final angle after springback, θ_f [10].

$$R_f = \frac{R_i}{4(\frac{R_i \sigma_y}{Et})^3 - 3(\frac{R_i \sigma_y}{Et}) + 1}. \tag{3.8}$$

It was determined from this equation that the maximum springback that could occur with the multipurpose stainless steel was 3.5 degrees, and therefore the mirror mount angular range from the stainless steel material was ± 1.75 degrees.

23
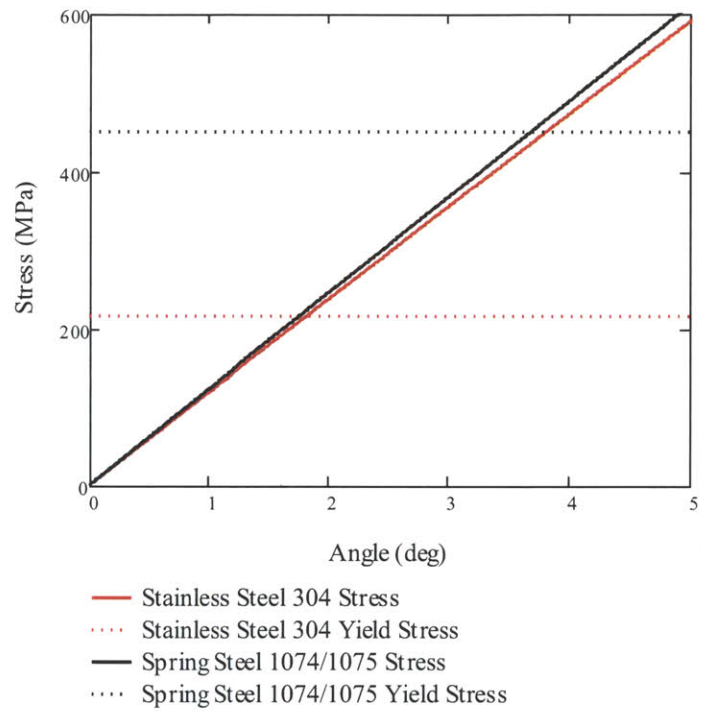
Figure 3-4: Flexure stress as a function of angle

Chapter 4

Design and Manufacturing

The Michelson interferometer assembly includes a laser and mount, a lens and mount, a beamsplitter and mount, two mirrors and mirror mounts, mounting material, and mounting brackets.

4.1 Optical Components

As shown in section 2.2, the Michelson interferometer is comprised of several different optical components, and each is held in place by an appropriate mounting device. Three main distributors of optical components, Newport Corporation, Thor Labs, and Edmund Optics, sell both optical components and optical mounts. However, these components are highly precise and sold at a markup, so the prices are relatively expensive for a student's budget. In addition, the sizes are too big and are incompatible with the MICA sensors.

The MICA optical components, including the laser, lens, beamsplitter cube, and mirrors, were optimally chosen by comparing the quality and the price of each. High quality components would increase the ease of obtaining a high resolution interference pattern; however, cost must be kept to a minimum in order to allow the Michelson interferometer kit to be obtained by students at a reasonable price.

4.1.1 Laser

In order to obtain a fringe pattern, the laser needs to have non-pulsed continuous operation, as well as a highly collimated beam diameter with small divergence. The color of the laser is not particularly important; however, a green (532 nm) DPSS laser was chosen due to its long coherence length. Coherence length corresponds to the maximum optical path difference at which the fringe pattern is still visible, and it can be estimated from measuring the largest difference in path length of two mirrors in a Michelson interferometer in which there is still a visible fringe form. With a long coherence length, the difference in path lengths can be large and there will be high fringe visibility with good contrast.

Two different green DPSS lasers were initially sought out by another researcher for this project, an internal module from LaserGlow's Galileo Series laser pointers, and a Quarton green laser module, purchased from Digikey. The price of the Laserglow laser was $40 while the other laser was approximately $100. Both laser modules were less than 15 mm in diameter and would be able to be mounted on the appropriate 25 mm × 25 mm laser mount. Measurements were made on each laser to compare their coherence lengths. The coherence length is given by twice the travel distance in which the fringes are visible, while moving one mirror in the Michelson setup [11]. In the experiment, one mirror was translated from its initial position of 25 mm to its final position of 800 mm with both lasers. It was concluded that the coherence length of each lasers was greater than 1.5 m. However, due to limited space, the "final position" was not yet the position at which the interference pattern disappeared, so the exact coherence length could not be determined. It was also observed that the Quarton laser had higher laser power.

After taking into consideration the results of this experiment, the similarity in other specifications such beam diameter and divergence, and the prices, the Laserglow laser was chosen for building the laser mount and obtaining the interference patterns. An alternative laser could also be used, simply by altering the geometry of the laser mount.

4.1.2 Lens

The Michelson interferometer utilizes a diverging lens, the most common type being a double concave lens. Size and focal length were considered when choosing an optimal lens. The lens had to be less than 20 mm in diameter to fit centered in the 25 mm square mount. The focal length needed to be negative such that the focal point was behind the lens to divert the collimated laser beam. Additionally, a shorter focal length diverges the collimate laser light source at a larger angle, producing a larger interference pattern. The diverging angle, θ, of a double concave diverging lens is given by the equation

$$\theta = \arctan \frac{d_{pattern}}{l_{path}}, \tag{4.1}$$

where $d_{pattern}$ is the diameter of the interference pattern and l_{path} is the path length the light traveled from the diverging lens to the viewing area. The focal length, f, is then determined from the equation

$$f = \frac{\frac{1}{2}d_{beam}}{\tan\theta}, \tag{4.2}$$

where d_{beam} is the diameter of the laser beam, or 1.5 mm. A sketch of the diverging lens geometry is shown in Figure 4-1. Given that the path length of the assembled Michelson interferometer is approximately 325 mm, and the approximate size of the desired interference pattern is 20 mm in diameter to fit on a 25 mm square screen, the desired focal length is approximately -12.2 mm. A double concave lens was used for $4.5 from an overstock warehouse, Surplus Shed, with a focal length of -12 and a diameter of 18.2 mm.

4.1.3 Beamsplitter cube

A beamsplitter cube is formed from two triangular prisms. The diagonal interface between the two prisms transmits part of the light and reflects the rest at a ninety degree angle. In a Michelson interferometer, it is necessary to have a beamsplitter
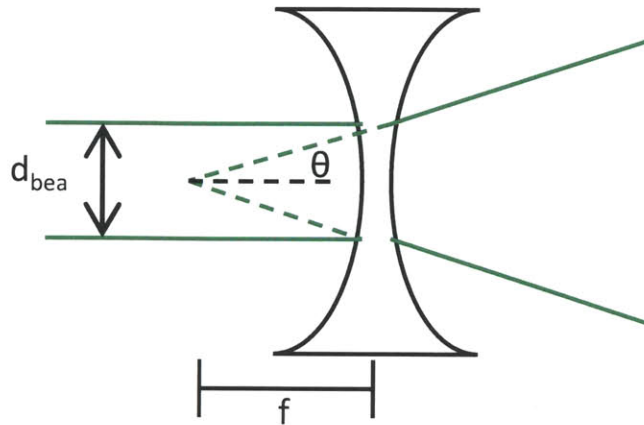
Figure 4-1: Geometry of diverging lens

that transmits 50-50, such that 50% of the light is transmitted and the other 50% is reflected. It is also important to have a high precision surface flatness so that incoming light is not reflected off the surface in any arbitrary direction. Again there is a trade-off between surface precision and cost. A standard 20 mm square beamsplitter was used to ensure that it would fit in a custom 25 mm square mount. The beamsplitter had high quality surface flatness and was the most expensive optical component in the assembly, costing around $200. Educational-quality beamsplitters at a much lower cost ($25) may potentially be used as well.

4.1.4 Mirrors

The mirrors are to be mounted on the mirror mount and are responsible for reflecting the light back towards the beamsplitter. Again, like the beamsplitter, the most important qualities are the size and the surface flatness. The mirror had to be less than 23 mm by 25 mm to fit on the front face of the mirror mount. The more precise the surface flatness is, the more precisely the light beam will be reflected directly back to the beamsplitter. To keep cost low, two mirrors from Surplus Shed were used. The mirrors were 22 mm square, 4.7 mm thick, and cost only $4.5 each. The surface flatness was not provided; however, it was determined from experiments that

28

the surface flatness was adequate for its educational purpose.

4.1.5 Mounting material

Normally, an interferometer is mounted on an optical table because it dampens external vibrations [6]. However, optical tables are extremely expensive, and not feasible for a low-cost MICA education project. Instead, black-anodized aluminum extrusions with a 25 mm square cross section and a 6 mm slot profile were used [12]. These aluminum extrusions and corresponding hardware allow the user to easily mount the optical component mounts to the extrusions.

4.2 Benchmarking Optical Mounts

Each component of the Michelson interferometer needs to be mounted and positioned appropriately. For a given component, the mount can either be stationary or have up to six adjustments, including translation in the x, y, and z directions as well as rotation in each of these axes. In either mentioned Michelson interferometer configuration, it is necessary to rotate the mirror mounts in two orthogonal axes in order to obtain precise perpendicular alignment [13]. The other component mounts, including the laser mount, lens mount, and beamsplitter mount do not require any degrees of freedom and can be stationary.

The same three main distributors were considered for the simpler mounts. Fixed lens mounts can be priced anywhere between $15 and $60, depending on the size of the lens diameter [14]. Newport's fixed laser mounts are priced at $90 [15], while Edmund's are priced at $165 [16]. Beamsplitter mounts can cost more than $50 [14, 15, 16].

Mirror mounts, which need to be adjusted for rotation in two axes, are also mainly distributed through Newport, Thor Labs, and Edmund. There are three types of mirror mounts on the market, including kinematic, flexural, and gimbal. Gimbal mounts, shown in Figure 4-2c, rotate the mounted mirror along the center axes while keeping the position of the center of the mirror stationary. This feature of keeping

29

the mirror center stationary is unnecessary for an educational Michelson. In addition, these mirror mounts tend to be more expensive, so they were not considered for the MICA Project [15]. Kinematic mirror mounts use small extension springs and a steel ball as shown in Figure 4-2a, to rotate along two axes. They are priced between $35 and $200 [14, 15, 16]. Lastly, flexure mounts are not as common, as they are only available through Newport, but also achieve two-axis tilt and are priced around $100 [15].
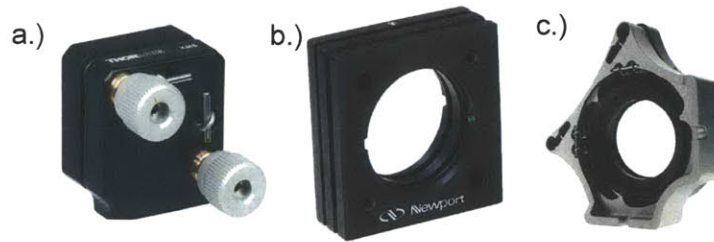
Figure 4-2: Three types of mirror mounts available on the market. a.) Thor Lab's Compact Kinematic Mount [14] b.) Newport's Flexure Industrial Optical Mount [15] c.) Newport's Ultima Gimbal Center Mirror Mount [15]

Table 4.1 details key specifications and prices of mirror mounts with two axis adjustments available through the three distributors.

Table 4.1: Comparison of price and specifications of mirror mounts from three key distributors

Mirror Mount	Specifications			Price
	Adjustment screw pitch	Drive type	Angular range	
Edmund: Small Angle Mirror Mount	0.4 mm	Knob	±10 deg	$49
Thor labs: Compact Kinematic Mirror Mount	0.25 mm	Knob	±4 deg	$34
Newport VIZIX (Kinematic) Mirror Mount	0.25 mm	Knob	±4 deg	$40
Newport Flexure Mirror Mount	0.32 mm	Allen Key	±2.5 deg	$99-$106

To conclude, benchmarking and cost-analysis demonstrates that it would cost

30

around $450 dollars to configure an optical system from the main distributors that would be suitable for a Michelson interferometer educational kit, which is far too expensive. However, the designs and manufacturing methods presented in the subsequent sections, present an alternative that achieves the educational goals of the MICA optical module while maintaining much lower costs.

4.3   Mirror Mounts

4.3.1   Design Process

As mentioned in section 4.2, two mirror mount designs were considered and compared, a kinematic design and a flexural design. The kinematic design is the most common and usually costs less than other designs. It consists of only two aluminum plates, one fixed and one moveable. The moveable plate is constrained by a steel ball in one corner and two ball-ended adjustment screws in two other corners. The plates are held together by extension springs, preventing motion in all six degrees of freedom. Torsional springs could be used in place of the extension springs, but may cause expansion rather than tilt. The two adjustment screws can be fine-pitched screws or micrometers, and function to tilt the moveable plate on the mirror mount [13, 17, 18, 19]. An image of the kinematic CAD model is shown in Figure 4-3. Although this design is common and widely available, it also includes a large number of parts and consequently incur high material and assembly costs, outlined in Table 4.2.
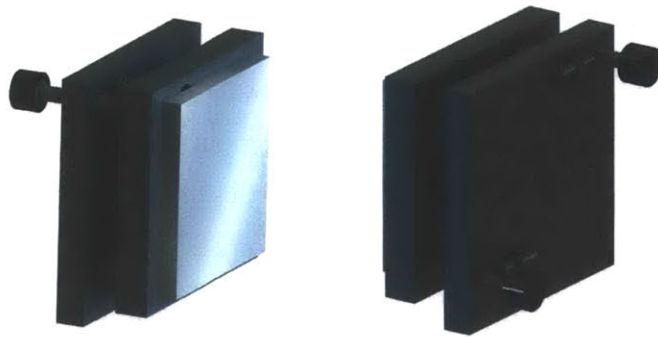

Figure 4-3: CAD assembly of kinematic mirror mount

31

Flexural designs were also considered. Flexural mirror mounts are only available through Newport at a price of $100. This design consists of three aluminum plates. The back plate is fixed and is connected to the middle moveable plate along its side face by a thin piece of metal, or a flexure, as discussed in 3.2. The middle plate is then connected to the moveable front plate by another flexure along the bottom face. There are also two adjustment screws. One adjustment screws tilts the middle and front plate assembly around one axis and the second adjustment screw tilts the front plate around another axis. Figure 4-4 shows a flexural design that uses a bolting method to secure the flexure to the plates.

Figure 4-4: CAD assembly of flexural mirror mount

In addition to the three-plated two-flexure design, two-plated, single-flexure designs were explored to eliminate the cost of the extra middle plate. First, a multi-axis flexure was considered. This flexure geometry makes it fairly simple to manufacture, but the design was rejected because it would require additional components to resist twisting around the cylindrical axis. Second, a two-axis flexure was also considered. This design would allow for rotation along two axes, as the three plated design does. The thick material between the two bending portions would ensure that there was little stress concentration in the corner, but this design could cause expansion rather than tilt. CAD models of the multi-axis flexure designs are shown in Figure 4-5.

After consideration, the two-plated, single-flexure designs were not pursued due to their functional limitations, the advanced manufacturing methods, and the lack of specific improvements they might provide over the three-plated flexural design.
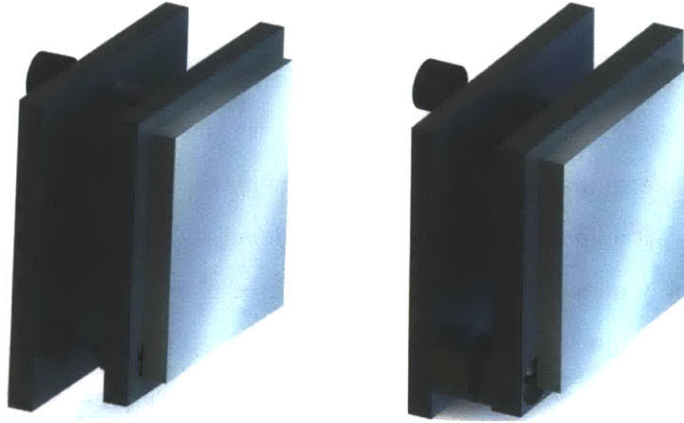
Figure 4-5: CAD assemblies of other flexural designs a.) multi-DOF b.) 2-DOF

Thus, the two main designs that warranted further analysis were the kinematic design and the three-plated flexural design. A summary of the costs of the kinematic and flexural designs is shown in Table 4.2.

Table 4.2: Part cost estimation of kinematic and flexural mirror mount designs

Kinematic				Flexure			
Material	Quan-tity	Unit Price ($)	Total ($)	Material	Quan-tity	Unit Price ($)	Total ($)
Aluminum 25×25×3 mm	2	0.10	0.20	Aluminum 25×25×3 mm	3	0.10	0.30
Adjustment screws: M2×8, M2×14	2	0.07	0.14	Adjustment screws: M2×8, M2×14	2	0.07	0.14
Steel ball	1	0.10	0.10	Spring steel: 8×22×0.5 mm	1	0.14	0.14
Aluminum rods or additional screws	4	0.01	0.04	Flexure screws	8	0.05	0.40
Extension springs	2	2.69	5.38				
Total			**5.86**	**Total**			**0.98**

The table shows that the deciding cost factor between the two designs was the

33

extension springs for the kinematic design, which contributed to about 90% of the cost of the kinematic design. This made the material cost of the kinematic design greater than 5 times the material cost of the flexural design. Therefore, as the two designs have similar functionality, the kinematic design was not pursued further.

Three attachments methods for the flexural design are possible, using screws to mechanically attach the flexures to the three plates, spot welding the flexures into a notch in the plates, and by wire EDM. First, the mechanical method using screws requires four to eight small screws and attachment points (holes in the flexure/plate) to attach the first flexure to the sides of the back and middle plates, and another four to eight small screws and attachment points to attach the second flexure to the bottom of the middle and front plates. This method is shown in Figure 4-4. Second, in the notched design, the flexures are attached to the plates by spot welding the flexures into notches in the plate. This design is implemented by Newport and can be seen in Figure 4-2b. The final design considered was a single part design. The entire mirror mount, including the plates and the flexures, are made out of a single block of material using the wire EDM. The CAD model of the EDM manufacturing method is shown in Figure 4-6.
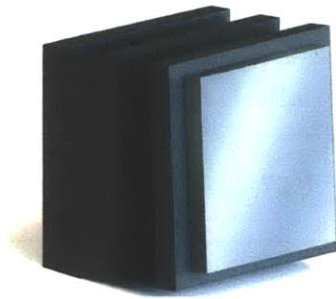
Figure 4-6: CAD model of flexural design with EDM manufacturing method

Each of the three attachment methods has distinct advantages and disadvantages. The mechanical attachment method is the simplest to prototype and has the least complicated manufacturing method. However, it requires many parts and a large number of assembly steps. With the mechanical attachment method, it is also possible to use different materials for the plates and the flexures, so the flexures could be made

out of spring steel, a material with high yield strength. Nevertheless, preloading the design to a negative angle during assembly is difficult and only possible with either geometrical changes to the plates or the use of magnets.

The notched method requires fewer parts and assembly steps than the first design, but it requires a relatively complicated and expensive manufacturing step, spot welding. It is again also possible to make the plates and flexures from different materials, and preloading is possible if the notches are made at slight inward angles.

The single part method using a wire EDM process is very expensive. However, the mirror mount could potentially be die cast to reduce cost at a high output level. The flexures are made out of the same material as the plates, which would be stainless steel or another castable metal with high yield strength. It would not have the extremely high yield strength of spring steel. However, it is simple to preload. Table 4.3 compares the different flexural mirror mount manufacturing options is shown below.

Table 4.3: Comparison of manufacturing options for the flexural mirror mount design. Using the mechanical attachment method as standard, "S" designates that the attachment method is similar to the mechanical method, while "+" and "-" refers to an improvement or a shortcoming of the method to the mechanical attachment method, respectively.

	Mechanical	Notched	EDM
Manufacturing Process	S	-	+
Flexure quality	S	S	-
Preload Ability	S	+	+
Aesthetics/ Simplicity for student	S	+	++
Cost	S	S	-
Total	S	+	++

4.3.2 Prototype and Final Design

Based on the factors in the design table, it was determined that the EDM design was superior to the other two designs. Although the mechanical design was not optimal

for high volume manufacturing, it was utilized for prototyping. Pending the successful completion of the prototype, the final design would be made from the EDM design. In the prototype, the plates were made from milling Aluminum 6061. The flexures were made from 1074/1075 spring steel approximately 0.45 mm thick. Eight circular cutouts were made in two small, 8 mm × 22 mm piece of spring steel using the wire EDM. Sixteen holes were drilled and tapped in the corresponding sides of the plates, four for each side of the two flexures. After assembly, the mirror mount could be tilted from 0 degrees to over five degrees and spring back to its original position around both axes. The mirror mount prototype is shown in the Figure 4-7.
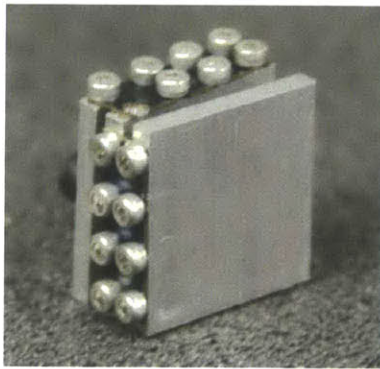

Figure 4-7: Image of the flexural mirror mount prototype

After the prototype proved the concept viable, the mirror mount was then designed and manufactured using wire EDM. The CAD model uses two extruded cuts, while keeping the middle plate aligned with the coordinate system. This was done to avoid making any angled cuts with the wire EDM, which would be necessary if either the front or the back plate was aligned with the coordinate system. In the first version, the flexures were 300 μm thick and the plates were preloaded to -2.5 degrees. This version was then made by wire EDM. Starting from a bar of multipurpose stainless steel with a 31.75 mm square cross section, the front plate was cut first. The block was then rotated ninety degrees, and the back plate was cut to finish the part. The M1.6 mounting hole and the two M2 adjustment screw holes were manually drilled and tapped. However, after this version was completed and tested, it seemed to be too weak, and adjusting the mirrors caused small vibrations. Also, since stainless

steel rather than spring steel was used, the mirror did not spring back to its original position due to plastic deformation.

In the second and final version, the flexure thickness was increased from 300 μm to 350 μm to increase the stiffness. Also, the plates were preloaded further in order to allow for adequate springback. The final part is shown in Figure 4-8.
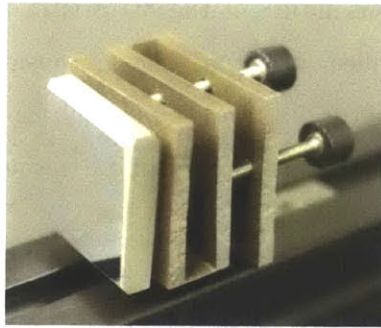

Figure 4-8: Image of the final flexural mirror mount

4.4 Additional Components

4.4.1 Laser Assembly

The laser mount was designed to have a 25 mm square face with a 4 mm thickness. The circular opening must be centered and correctly sized for the laser. The front section of the laser from LaserGlow had a 7.48 mm diameter. Therefore, the circular opening was made to be 7.58 mm, allowing for 0.1 mm of clearance. The laser mount was cut using the wire EDM. First, a small hole was drilled in aluminum 6061 stock. The wire was then threaded and centered in that hole and widened to the appropriate diameter. Next, the wire was moved outside the hole, rethreaded, and the 25 mm square outline of the mount, including the M1.6 hole, was cut. An M3 sized hole was drilled and tapped from the top of the mount into the circular opening. An M3 setscrew constrains the laser in the circular opening. A M1.6 sized hole was placed 1.5 mm from the bottom and centered across the width. The laser mount is mounted to the aluminum extrusions via a M1.6 low-profile head screw and modified blind

brackets, which are discussed in section 4.4.4.

Since the laser was purchased as an "internal module," the electronics were exposed. For safety reasons, it was necessary to implement a cap, or simply a tube with an opening in the back for the wires, to cover the exposed electronics. The rest of the laser had an 11 mm diameter. The cap was made to have an 11.4 mm inside diameter. Because of the nature of the 3D printer and the resin, a designed 11.4 mm inside diameter yielded an actual 11.3 mm inside diameter. This left 0.3 mm of clearance between the cap and the laser, resulting in a loose fit. The cap can be adjusted for the size of the laser or for a more permanent press-fit. The final laser assembly is shown in Figure 4-9.
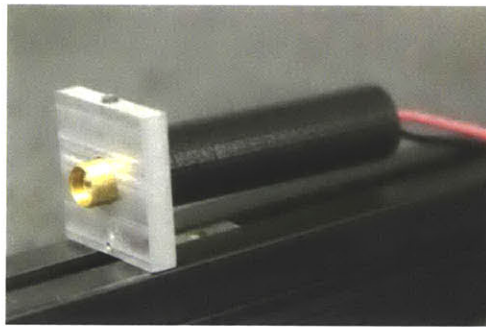

Figure 4-9: Image of final laser assembly

Currently, the power and ground wires are soldered to the electronics underneath the cap, and the laser is powered directly from a 3.0 V power supply. For full-scale manufacturing, a battery pack can be included in the laser assembly.

4.4.2 Lens Mount

The lens mount was designed and built similarly to the laser mount. It has a 25 mm square face and 4 mm thickness. The circular opening in the center of the face is 18.32 mm in diameter to leave 0.1 mm clearance for the 18.22 mm diameter lens. It was manufactured by the wire EDM using the same steps described with the laser mount, but adjusted for the size of the center opening. However, for the lens assembly, the set screw that constrained the lens was nylon tipped in order to reduce the chance of

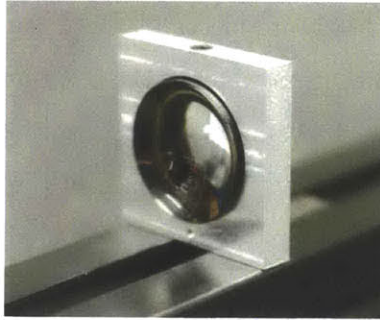cracking the lens. The final lens assembly is shown in Figure 4-10.

Figure 4-10: Image of final lens assembly

4.4.3   Beamsplitter Assembly

The beamsplitter assembly was designed as a 25 mm cube. Top and the bottom plates are 2.5 mm thick, and they are held together by pillars in two corners. The top and bottom plates of the beamsplitter assembly were manually milled to the correct size out of standard aluminum 6061 stock. The pillars, made using the wire EDM, are 10 mm in length with a cross section containing an inside corner. This inside corner constrains the 20 mm beamsplitter cube. M2 holes were drilled and tapped on either end of the pillars, and counterbore holes were drilled in the top and bottom plates to recess the M2 screws. Again, the M1.6 mounting hole was drilled and tapped. The final beamsplitter assembly is shown in Figure 4-11.
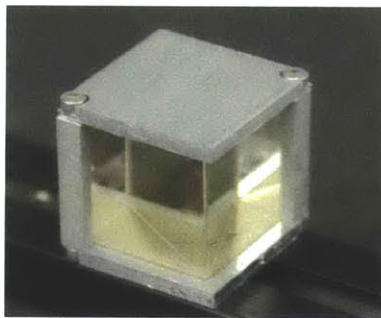

Figure 4-11: Image of final beamsplitter assembly

4.4.4 Modified Misumi Blind Bracket

Misumi supplies several hardware pieces for the 25 mm square aluminum extrusions discussed is section 4.1.5. One of which is the blind bracket, which is used to connect two aluminum extrusions at a ninety degree angle. It has a profile that locks into the extrusions' top slot so that the top face of the bracket is flush with the top face of the extrusions. These blind brackets were modified to function as brackets for mounting the optical mounts on the extrusions. Using the wire EDM, the small inside radius was faced to create a sharp right angle, and one leg of the right angle was cut shortened, leaving 3.5 mm of material between the inside corner and the new top. This shortened side was used to connect the mount to the bracket, and the longer side was constrained inside the aluminum extrusions. Next, a hole was made on the shortened side, which was tapped to fit the M1.6 mounting screw. Finally, the face that becomes flush with the optical mount was faced to be perpendicular to the top face of the aluminum extrusion. This was a necessary step to ensure that all of the optical mounts were parallel so that the laser light would travel along a straight path. A before and after picture of the bracket is shown in Figure 4-12.

Figure 4-12: Image of Misumi's blind bracket and the modified blind bracket

Chapter 5

Results

Interference patterns were obtained from two different configurations. In the first configuration, the lens was placed on the other side of the beamsplitter after the light paths had recombined, which yielded a straight line interference pattern. In the second configuration, the lens was placed directly after the laser and before the beamsplitter, which resulted in a circular pattern of interference. The fringes are each a little larger than 20 mm in diameter, and are approximately 150 mm away from the beamsplitter. The final assembly of the MICA Michelson interferometer and the interference patterns are shown in Figure 5-1.
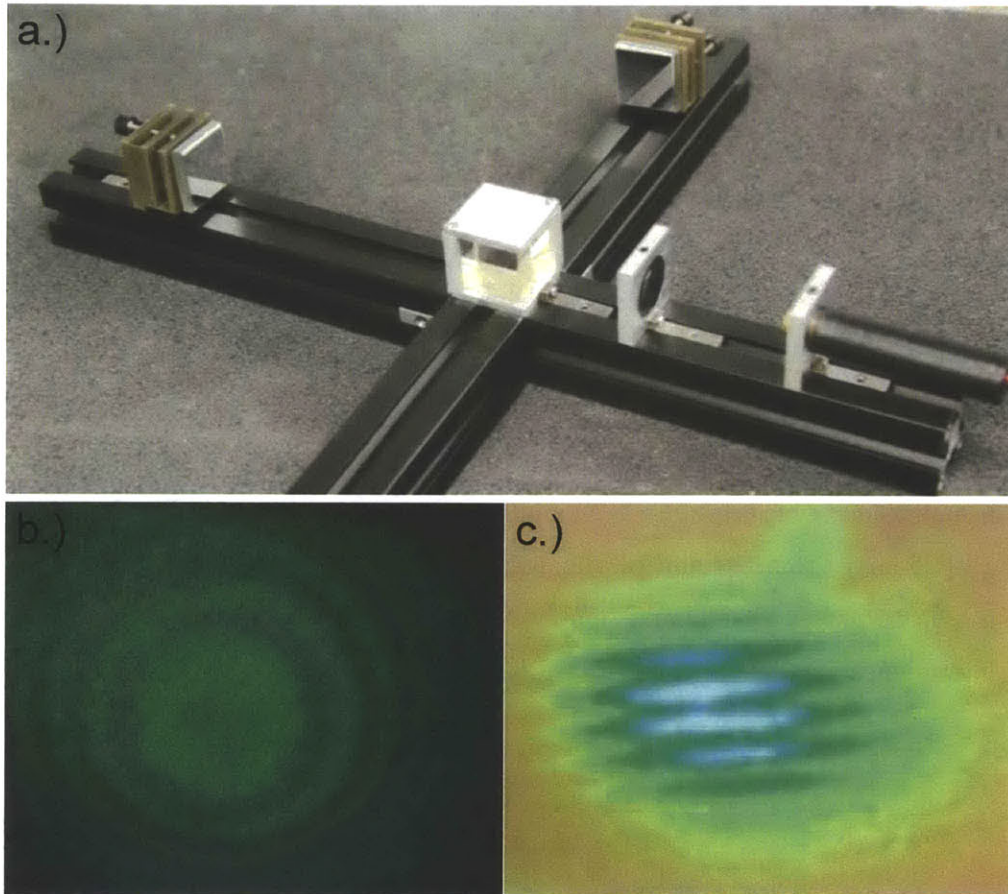
Figure 5-1: a.) Image of the MICA Michelson interferometer assembly b.) Circular fringes obtained from first configuration with lens in front of the beamsplitter. c.) Straight line fringes obtained from second configuration with lens behind the beamsplitter

Chapter 6

Conclusions and Recommendations

With careful and cost-conscientious design, the MICA Michelson interferometer and corresponding optical laboratory experiments can become affordable for online students. By obtaining low-cost optical components discussed in section 4.1 and manufacturing each component mount to cost approximately $5 utilizing economies of scale, the Michelson interferometer module would cost only around $100, about the cost of science and engineering textbooks. Several laboratory experiments can be completed using only the stationary interferometer components developed in this thesis. First, by correctly assembling and aligning the components, students learn about the properties of each optical component. For example, with the beamsplitter, students learn about the properties of the two prisms and the resulting 50-50 light paths. With the diverging lens, they learn about the relationship between focal length and beam angle. Furthermore, by correctly aligning the components in different configurations students can obtain interference patterns and learn about basic interferometry, after the corresponding theoretical calculations. The students may also measure coherence length if provided with a red laser with a shorter, measurable coherence length.

The MICA Michelson interferometer could be improved by altering the mirror mount's material and design. Currently, the mirror mounts have enough angular range to correctly align the laser beams to produce an interference pattern, as shown in Figure 5-1. However, due to the material properties of multipurpose stainless steel, the flexures deform plastically and rely on springback to return the plates to a negative

43

angle. By changing the material to one with higher yield strength, the flexure would have a larger elastic regime, thus increasing the angular range of the mirror mounts. Furthermore, the mirror mount was manufactured using the wire EDM under the assumption that a lower-cost method, such as die casting, could replace the wire EDM in high volume manufacturing. If casted, it would not be possible to implement higher yield strength, but would result in a significantly lower cost.

Kinematic components and sensors could further this project. By adding a precision micrometer stage to one of the mirror mounts, the wavelength of the laser light can be measured by counting the number of fringe changes on the interference patterns. Another simple experiment could be the measurement of the thermal expansion coefficient of aluminum or another metal. By heating up a rod of aluminum, and simultaneously measuring the change in distance via fringe changes with a photodetector and the change in temperature of the rod, the thermal expansion coefficient can be obtained. In another experiment, by introducing a motorized mirror mount and adding a MICA photodetector sensor that counts the fringe changes, students would potentially be able to graph their results and learn about fast Fourier transforms [20].

To conclude, this thesis outlined the development of the MICA Michelson interferometer, which provides an inexpensive optics module to the MICA Project. The range of possible experiments with this module can be extended with the addition of movable components and other MICA sensors. Overall, the MICA Project directly complements current online educational initiatives by coupling theoretical understanding with hands-on experiments.

Bibliography

[1] P.C. Wankat and F.S. Oreovicz. *Teaching Engineering*. McGraw Hill, New York, 1993.

[2] edx. [Online] Available: https://www.edx.org/ [Accessed: April 17, 2013].

[3] Brian D. Hemond, Adam Wahab, Adam Spanbauer, Ian W. Hunter, Barbara J. Hughey, and Lynette A. Jones. MICA: An innovative approach to remote data acquisition. *IEEE Instrumentation & Measurement Magazine*, 15(5):22–27, 2012.

[4] Eugene Hecht. *Optics*. Pearson Education, San Francisco, 4th edition, 2002.

[5] Max Born and Emil Wolf. *Principles of Optics*. Cambridge University Press, New York, 7th edition, 1999.

[6] P. Hariharan. *Basics of Interferometry*. Academic Press, Boston, 1992.

[7] A.A. Michelson. *Studies in Optics*. Phoenix Books, Chicago, 1963.

[8] Albert Michelson and Edward Morley. On the relative motion of the earth and the luminiferous ether. *American Journal of Science*, 34(203):333345, 1887.

[9] Stuart T. Smith. *Flexures : Elements of Elastic Mechanisms*. Gordon & Breach, Amsterdam, 2000.

[10] Vukota Boljanovic. *Sheet Metal Forming Processes and Die Design*. Industrial Press, New York, 2004.

[11] Milton Katz. *Introduction to Geometrical Optics*. World Scientific Publishing, Singapore, 2002.

[12] Misumi USA, Inc. Mechanical standard components for factory automation. Catalog, 2010-2011. [Online] Available: http://us.misumi-ec.com/ [Accessed: April 28, 2013].

[13] John H. Moore, Christopher C. Davis, Michael A. Coplan, and Sandra C. Greer. *Building Scientific Apparatus*. Cambridge University Press, New York, 2009.

[14] Thor Labs, Inc. Thor labs v21. Catalog. [Online] Available: http://www.thorlabs.com/ [Accessed: April 28, 2013].

[15] Newport Corporation. Newport resource. Catalog, 2011/2012. [Online] Available: http://www.newport.com/ [Accessed: April 28, 2013].

[16] Edmund Optics. Optics and optical instruments master source book. Catalog. [Online] Available: http://www.edmundoptics.com/ [Accessed: April 28, 2013].

[17] Sechrist et al. Precision Optical Mounts, U. S. Patent 5,757,561, May 26, 1998.

[18] Nunnally et al. Optical Mount with a Locking Adjustment Screw, U.S. Patent 6,016,230, January 18, 2000.

[19] Sechrist et al. Precision Opical Mounts, U.S. Patent 6,304,393, October 16, 2001.

[20] B.J. Hughey and I.W. Hunter. 2.671 measurment and instrumentation laser interferometer experiment procedure. 2.671 Laboratory Instructions, MIT, Spring, 2012, 2012.